PHYSICAL REVIEW E **88**, 031101(R) (2013)

Thermal energy density of dust in dusty plasmas: Experiment and theory

R. Fisher,[1] K. Avinash,[2] E. Thomas,[1] R. Merlino,[3] and V. Gupta[2]
[1]*Physics Department, Auburn University, Auburn, Alabama 36849, USA*
[2]*Department of Physics and Astrophysics, University of Delhi, Delhi-7, India*
[3]*Department of Physics and Astronomy, The University of Iowa, Iowa City, Iowa 52242, USA*
(Received 13 April 2013; published 23 September 2013)

A surprising observation in dusty plasma experiments is that the dust thermal energy density, $P_d \propto n_d T_d$, is typically much greater than $n_d T_n$ (where n_d and T_d are the dust density and temperature, and T_n is the neutral temperature), even though the dust particles would be expected to be in thermal equilibrium with the neutrals. We show here, theoretically and experimentally, that the anomalously high dust thermal energy density can be accounted for if electrostatic interactions between the dust particles and the background plasma are taken into account. Thus, the dust pressure in dusty plasma is mostly of electrostatic origin.

DOI: 10.1103/PhysRevE.88.031101 PACS number(s): 52.27.Lw, 52.25.Kn

I. INTRODUCTION

A dusty plasma is an electron-ion plasma which contains a dispersed phase of micron and sub micron sized particles called dust grains. In the plasma environment these particles acquire a large negative charge ranging from 10^3 to 10^4 electronic charges, depending on the size of the dust. The presence of this large charge on the dust introduces new processes and phenomena in the plasma; some of these are the dust acoustic waves [1,2], strongly coupled two-dimensional (2D) and three-dimensional (3D) crystalline states, and moderately coupled liquid states of dust particles [3–6]. Since dust particles are typically large they can be imaged directly with video cameras. This has given a unique opportunity to researchers to study a number of fundamental thermodynamic issues at the kinetic level, e.g., phase transition, phase coexistence, freezing and melting dynamics, and transport of dust grains in dusty plasma.

Recently developed imaging techniques are revealing details about the structure and dynamics of dusty plasmas [7–9]. In particular, two-dimensional and stereoscopic particle image velocimetry (PIV) has led to a direct measurement of full 3D distribution functions in the configuration and velocity space of dust particles in dusty plasmas [10,11]. This diagnostic measures average velocity vectors for small groups of particles in a plane that is illuminated by pairs of laser pulses. The main advantage of this technique is its quick ability to reconstruct the particle positions and velocities accurately over the entire field of view of the cameras. Using this diagnostic, Thomas and co-workers have made detailed measurements of thermodynamic properties of the dust component in weakly coupled dusty plasmas [12,13].

The PIV data show some interesting observations; e.g., the dust velocity distribution function is not spherically symmetric. In fact it is found that the trinormal distribution provides a much better fit to the data [14,15]. Hence the second rank pressure tensor of the dust is calculated by fitting the data with a trinormal probability distribution function instead of an isotropic Maxwellian distribution function. The trace of this tensor is the thermal energy density or the scalar pressure of the dust P_d.

Normally under quiescent conditions it is reasonable to assume that the kinetic properties of the dust are in equilibrium with the neutral background gas (cold dust), in which case $T_d \sim T_n$ and $P_d \sim n_d T_d \sim n_d T_n$ [here T_n and T_d are neutral and dust kinetic temperatures (the dust temperature T_d is distinct from the dust surface temperature) while n_d is the dust number density]. Surprisingly, it is found that the experimentally measured dust thermal energy density, P_d, is much greater than this estimate. In fact, the dust thermal energy density is of the order of ion thermal energy density even though the ion number density is much bigger than that of the dust. This is consistent with similar observations from other dusty plasma experiments which have revealed anomalously high dust temperatures [9,12,13,16–18]. However, the dust velocity distribution function is not spherically symmetric; furthermore it has been shown in Ref. [19] that a large value of dust temperature does not always correspond to a large value of energy density. Hence it has been argued that the dust thermal energy density P_d, instead of the dust temperature T_d, is a more appropriate measure of the dust thermal energy content of the dusty plasma. The excess dust thermal energy density of the dust component is the focus of this Rapid Communication.

Here, we show that the observed excess dust thermal energy density is due to the electric fields in the plasma background in the dusty plasmas. Typically in dusty plasma experiments, the dust cloud of volume V_d is confined within plasma of volume V ($V_d < V$). We calculate the dust free energy including electrostatic contributions from the plasma background in this case. For typical experimental parameters these electrostatic contributions are larger than the usual kinetic contributions. This may sound somewhat counterintuitive as it is generally believed that the electrostatic (ES) field contributions to the free energy are zero for dusty plasmas in the weakly coupled fluid limit. The ES contributions arise solely due to finite dust correlations effects in the strong-coupling limit. This is indeed true in the case of electron-ion plasmas (without dust) where the free energy is given by $F = F_{id} - (8/3)\sqrt{(\pi/2T)}e^3 n_p^{3/2}$ [20,21], where e is the electronic charge, n_p is the plasma density, and T is the temperature. Here the first term is the ideal gas (kinetic) contribution while the second term gives ES contributions due to electron and ion correlations. These contributions are of the order of g (g is the inverse of the number of particles in the Debye sphere) and hence are zero in the weak-coupling limit [20]. Here we show that in the case of dusty plasmas, such electric field contributions are

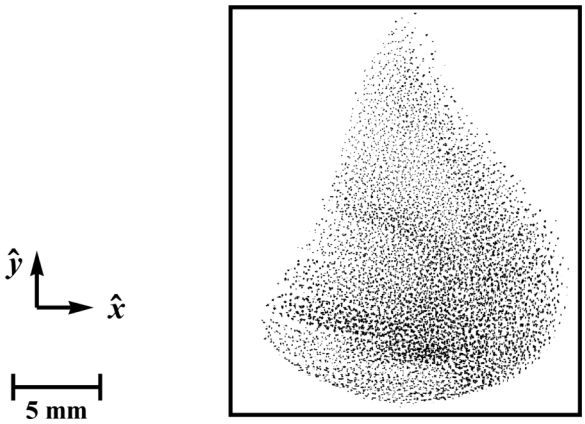

FIG. 1. A full camera frame view (color-inverted) of a dust cloud cross section in the 3DPX device.

finite even in the weak-coupling limit and are dominant over kinetic contributions. Thus the dust pressure in dusty plasma is mostly of electrostatic origin. This is one of the fundamental differences between dusty plasmas and electron-ion plasmas.

II. EXPERIMENT

The experiments to measure the dust thermal energy density were performed in the Auburn three-dimensional Dusty Plasma Experiment (3DPX) device. This is a dc glow plasma device which has been described in detail elsewhere [11,19]. It consists of two chambers of overall length of 75 cm and inner diameter of 10 cm. An argon plasma is generated in the experimental part of the chamber when an anode is biased at 200–250 V with respect to the grounded vacuum vessel and collects a discharge current in the range 2–5 mA. Spherical silica dust particles (with diameters of $3.0 \pm 1.5\ \mu$m) are introduced by placing a 5-mm-thick sheet of particles on the metallic surface below the anode. In the presence of the plasma, the dust particles become negatively charged due to thermal fluxes of ions and electrons and become levitated in the plasma. A dust cloud is thus formed in the plasma between the anode and the metallic plate. A picture of the dust cloud is shown in Fig. 1. Typical plasma parameters measured for similar discharges in 3DPX in the absence of the dust are the plasma density $n_p \approx 10^{14}$ m^{-3}, electron temperature $T_e \approx 4$ eV, and ion temperature $T_i \approx 1/40$ (assumed) $\approx T_n$.

The dust particles are diagnosed by illuminating them with laser sheet light in the x-y plane and the scattered light is recorded using a video camera. The 3DPX experiment is equipped with stereo-PIV diagnostic for imaging the dust grains. This technique determines velocity by finding the displacement of small groups of particles between two short laser pulses which are temporarily separated. Using this diagnostic it is possible to quickly reconstruct the position and velocity field over an entire field of view. To make these measurements, the experiment was filled with argon gas at a pressure of 132 mTorr, and a constant discharge current of approximately 5 mA was maintained with appropriate anode bias. The dust cloud was imaged using stereo PIV, after it had come to equilibrium following a period of formation and stabilization. Then 1500 PIV measurements were taken of each cloud cross section, with a laser pulse separation time of 500 μs, followed by 1500 measurements with a pulse separation time of 0.6 μs (for uncertainty quantification with the so-called zero displacement test).

After the two sets of PIV measurements were recorded for a given spatial cross section the translation stage carrying the PIV laser and cameras was moved 2 mm horizontally along the z axis and the process was repeated for all of the planes of constant $\hat{z}$ that were observed to contain dust. In total there were 13 such cross sections resulting in a total of 39 000 PIV "snapshot" measurements across the entire dust cloud structure. Each PIV measurement contained 330 velocity vector measurements (for a total of ~12 900 000 vectors) and a total of approximately 156 000 camera images. The average dust number density was measured by counting the average number of particles in a single volume element and dividing by the volume which gives $n_d \approx 10^{10}$ m^{-3}. The dust charge estimated from orbital motion limited (OML) theory was $q_d \approx 4400\, e$.

The result of velocity measurement using PIV gave two data sets from each volume element. The first data set of 1500 velocity vectors was used to construct 3D velocity distribution function while the second data of 1500 velocity vectors was used to quantify the error in velocity measurement. The measured velocity distribution functions were modeled by two continuous distribution functions; an isotropic 3D Maxwellian distribution function and an anisotropic trinormal distribution function. The parameters (the drift velocity vector field $\vec{u}_d$ and the velocity covariance tensor field $\overline{\overline{\Sigma}}$) of these distribution functions were calculated from the data. It was found that the velocity distribution function is anisotropic, and trinormal distribution given by Eq. (1) provides a better fit to the data [14,15,19].

$$F_T(\vec{v}) = (2\pi)^{-3/2}|\overline{\overline{\Sigma}}|^{-1/2} \times \exp\left[\frac{-1}{2}(\vec{v}-\vec{u}_d)^T \cdot \overline{\overline{\Sigma}}^{-1} \cdot (\vec{v}-\vec{u}_d)\right]. \quad (1)$$

The dust thermal energy density or the dust scalar pressure P_d is the trace of the pressure tensor and is given by

$$P_d = \tfrac{1}{2} n_d m_d \mathrm{Tr}(\overline{\overline{\Sigma}}). \quad (2)$$

As stated earlier P_d is a better parameter to quantify the energy content of the dust component. The experimentally measured thermal energy density of the dust throughout the cloud is shown in Fig. 2. The color scale and the approximate values for the other plasma components are, again, indicated in the histogram to give an idea of the scale of the dust component thermal energy density. From this figure it can be seen that in most of the cloud the dust thermal energy density P_d is a few times 10^{12} eV/m^3. In most dusty plasma experiments the dust is usually collisionally coupled with neutrals at room temperature in which case dust temperature $T_d \approx T_n = 1/40$ eV. Then, according to this estimate, with $n_d \approx 10^{10}$ m^{-3}, the dust thermal energy density would be of the order $\sim n_d T_n \sim 2 \times 10^8$ eV/m^{-3}. This is four orders of magnitude smaller than the experimentally observed value of $\sim 10^{12}$ eV/m^3. In fact, the dust thermal energy density is of the order of ion thermal energy density which is again surprising considering the fact that in glow discharges ion temperature

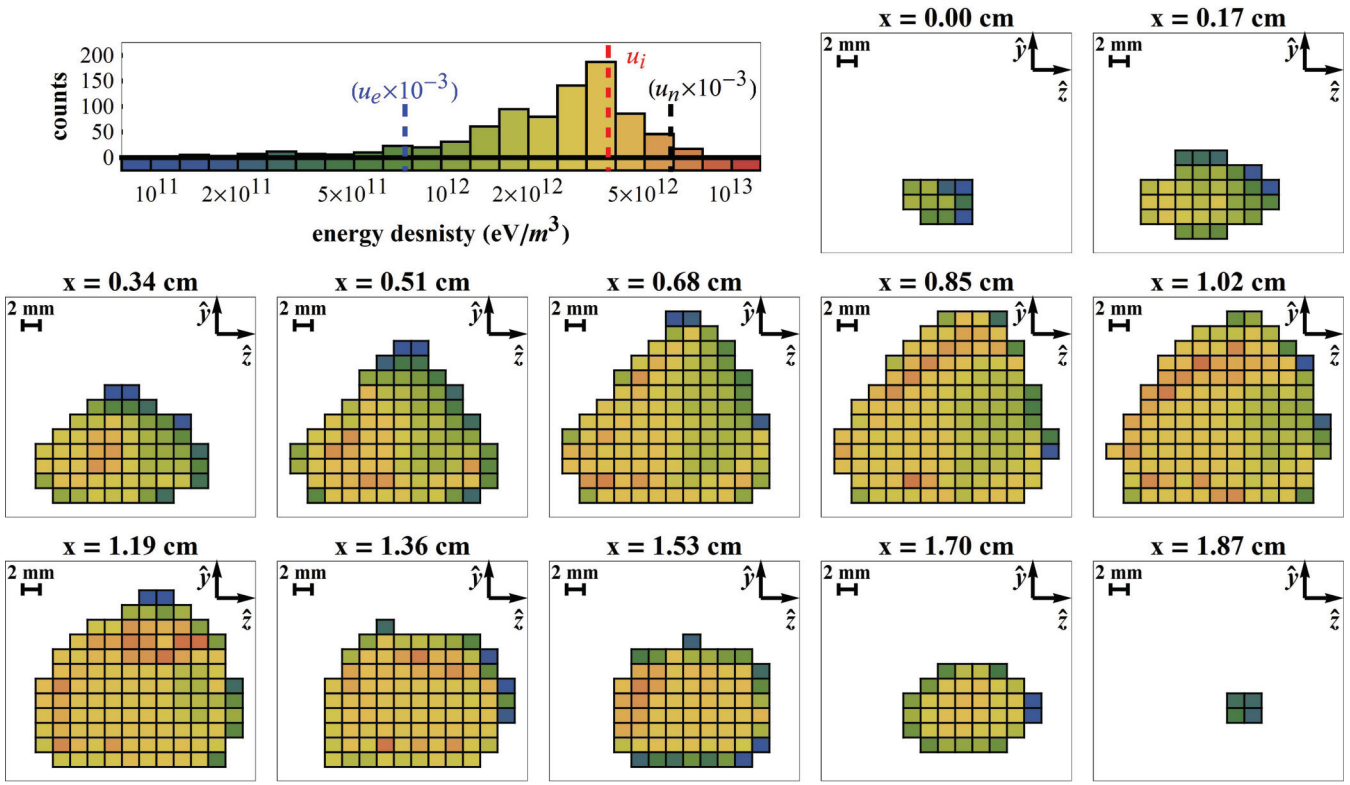

FIG. 2. (Color online) Thermal energy density. Histogram showing the energy density values calculated throughout the cloud attributable to the width of the velocity distribution. The energy densities are shown on a logarithmic scale. The average approximate thermal energy densities of the ion (u_i), electron (u_e), and neutral (u_n) plasma populations, multiplied by the indicated scaling factor, are indicated on the histogram for scale. The scalar field plots show the spatial distribution of the energy density using the same color scheme that was used in the histogram.

T_i is roughly equal to the neutral temperature T_n, and that ion number density n_i is much higher than n_d.

It should be noted that for these measurements the glow discharge was carefully operated in a stable parameters space where the dust cloud was quiescent and free of waves, mass flows, or any other type of nonequilibrium process which may heat the dust. In the next section we suggest an explanation of the observed excess thermal energy density of dust.

III. THEORY

In this part of the letter we calculate the free energy of dusty plasma F including the ES contributions from the plasma background. We show that they are dominant even in the weak-coupling limit and are enough to account for the excess dust pressure seen in experiments.

We start our calculations by considering N_d dust particles each carrying a negative charge q_d dispersed within a neutralizing plasma background which contains N_e electrons and N_i ions such that there is overall quasineutrality in the plasma volume V, i.e., $q_d N_d = e(N_i - N_e)$. As stated earlier in dusty plasma experiments, the dust is usually confined in a cloud of volume V_d, within plasma volume V by a suitable configuration of ES fields and forces.

Under the quiescent condition of the dust cloud we carry our calculations in the spirit of canonical ensemble theory where all three species possess given temperatures T_α where α denotes ion, electron, or dust species [19]. The electron and ion densities within the cloud are given by Boltzmann's relations. In the limit $q\varphi/T_e < 1$, these densities are given by $n_i = n_0(1 - e\varphi/T_i), n_e = n_0(1 + e\varphi/T_e)$ where $n_i = n_e = n_0$, and $\varphi = 0$ away from the cloud (φ is the ES potential). In the cloud the dust charge q_d is screened by the plasma electrons and ions. The ES potential at location r due to N_d screened dust particles is given by

$$\varphi = (-q_d/4\pi\varepsilon_0)\sum_j^{N_d} \frac{\exp(-\kappa_d|r - r_j|)}{|r - r_j|}, \tag{3}$$

where j^{th} dust particles are located at r_j and λ_d is the linearized Debye length given by $\kappa_d^2 = 1/\lambda_d^2 = (e^2 n_0/\varepsilon_0)(1/T_e + 1/T_i)$. The free energy F of the dusty plasma is given by $F = U - \sum_\alpha T_\alpha S_\alpha$ where U is the total internal energy of the system and S_α is the entropy of the α^{th} species. Now, in the fluid limit, the ES contributions to U are zero and are given by $U = \sum_\alpha (3/2)N_\alpha T_\alpha$ [20,21]. This has also been shown by explicit calculations [22]. Next, the entropy of the α^{th} species is given by [20]

$$S_\alpha = (5/2)N_\alpha - \sum_\alpha \int n_\alpha \left(\ln n_\alpha \Lambda_\alpha^3\right) dr,$$
$$\Lambda_\alpha^3 = \left(\frac{h^2}{2\pi m_\alpha T_\alpha}\right)^{3/2}, \tag{4}$$

In the expressions for the entropies of electrons and ions we substitute $n_i = n_0(1 - e\varphi/T_i)$ and $n_e = n_0(1 + e\varphi/T_e)$.

Expanding the log function in powers of $e\phi/T_e$, $e\varphi/T_i$ and retaining terms of order $(e\phi/T_e)^2$, $(e\varphi/T_i)^2$ we obtain

$$\sum_\alpha T_\alpha S_\alpha = \sum_\alpha \frac{5}{2} N_\alpha T_\alpha - \sum_\alpha N_\alpha T_\alpha \ln\left(n_\alpha \Lambda_\alpha^3\right) - \frac{\varepsilon_0 \kappa_d^2}{2} \int \varphi^2 dr. \quad (5)$$

In this equation, the first two terms give the usual kinetic contributions of all the species, while the last term contains the ES contributions of electrons and ions. The last integral can be evaluated by substituting the expression for φ from Eq. (3) with the result [22]

$$\sum_\alpha T_\alpha S_\alpha = \sum_\alpha (5/2)\, T_\alpha N_\alpha - \sum_\alpha N_\alpha T_\alpha \left(\ln n_\alpha \Lambda_\alpha^3\right) - \frac{q_d^2 \kappa_d}{16\pi\varepsilon_0} \sum_i \sum_j{}' \exp(-\kappa_d |r_i - r_j|). \quad (6)$$

The fluid limit of the last term can be extracted by replacing the double summation by smooth integration as $\sum_i \sum_j = n_d N_d \int_{V_d} dV_d$. Carrying out the double summations according to this prescription and substituting it in Eq. (6) we obtain the free energy F in the weak-coupling limit as

$$F = \sum_\alpha N_\alpha T_\alpha \left(\ln n_\alpha \Lambda_\alpha^3 - 1\right) + \frac{q_d^2 N_d^2}{2e^2 n_0 V_d} \frac{(T_e T_i)}{(T_e + T_i)}. \quad (7)$$

It is instructive to compare this expression with the corresponding expression of the free energy of electron-ion plasma (without dust) given by $F_{ei} = F_{th} - (8/3)\sqrt{(\pi/2T)} q^3 n_p^{3/2}$. In the weak-coupling limit, given by $q \to 0$, $n_p \to \infty$, and $en_p =$ constant, the ES contributions to F_{ei} approach zero while in F (in the corresponding limit) $q_d \to 0$, $N_d \to \infty$, these contributions are finite. Finally, the dust pressure P_d is given by

$$P_d = -\left.\frac{\partial F}{\partial V_d}\right|_{T_\alpha} = n_d T_d + \frac{q_d^2 n_d^2}{q^2 n_p} \left(\frac{T_e T_i}{T_e + T_i}\right), \quad (8)$$

where $n_p \approx 2n_0$ is the total plasma density. In Eq. (8), the first term gives the kinetic contributions to the total dust pressure from the dust at temperature T_d. The second term gives the ES contribution or the "electrostatic pressure" pressure of the dust. In 3DPX experiment $T_e \gg T_i \approx T_n \approx T_d$, taking this limit we obtain the total scalar dust pressure as $P_d = n_d T_d (1 + q_d^2 n_d / e^2 n_p)$. In 3PDX, $q_d/e \approx 4400$ and $n_d/n_p \approx 10^{-4}$; then with $n_d T_d \approx 2 \times 10^8$ eV/m^3, $P_d \approx 5 \times 10^{11}$ eV/m^3. This is within a factor of order unity of the experimental value (approximately a few times 10^{12} V/m^3) that is observed in the 3PDX device. Thus the electrostatic contributions to the dust scalar pressure are dominant over the kinetic contributions and are enough to account for the observed excess pressure. The scaling of the second term with dust volume ($\propto 1/V_d^2$) has been seen in recent numerical simulations.

IV. CONCLUSION

A calculation of the dust free energy has been presented earlier [22,23]. However, in these calculations the dust temperature T_d was taken to be zero and electron and ion temperatures were taken to be equal. Both of these conditions are not applicable to 3DPX experiment where the excess dust pressure has been observed. Here we have recalculated the free energy taking into account these effects.

In conclusion, the work presented in this Rapid Communication provides a straightforward theoretical model in combination with clear experimental evidence. The results show not only additional evidence for the anomalously high dust kinetic temperature, but also show that the electrostatic contribution from the background plasma to the total dust particle free energy is an important factor that must be included.

ACKNOWLEDGMENTS

Two authors (R.F. and E.T.) were supported with funding from the National Science Foundation through Grant No. PHY-0810419. One author (R.M.) was supported by DOE Grant No. DE-FG01-04ER54795.

[1] N. N. Rao, P. K. Shukla, and M. Y. Yu, Planet. Space Sci. **38**, 543 (1990).
[2] A. Barkan, R. L. Merlino, and N. D'Angelo, Phys. Plasmas **2**, 3563 (1995).
[3] J. H. Chu and L. I, Physica A (Amsterdam) **205**, 183 (1994).
[4] H. Thomas, G. E. Morfill, V. Demmel, J. Goree, B. Feuerbacher, and D. Möhlmann, Phys. Rev. Lett. **73**, 652 (1994).
[5] Y. Hayashi and K. Tachibana, Jpn. J. Appl. Phys. **33**, L804 (1994).
[6] O. Arp, D. Block, A. Piel, and A. Melzer, Phys. Rev. Lett. **93**, 165004 (2004).
[7] M. Kroll, S. Harms, D. Block, and A. Piel, Phys. Plasmas **15**, 063703 (2008).
[8] B. Buttenschön, M. Himpel, and A. Melzer, New J. Phys. **13**, 023042 (2011).
[9] M. Himpel, C. Killer, B. B. Buttenschön, and A. Melzer, Phys. Plasmas **19**, 123704 (2012).
[10] E. Thomas, Jr., Phys. Plasmas **6**, 2672 (1999).
[11] E. Thomas, Jr., J. Williams, and J. Silver, Phys. Plasmas **11**, L37 (2004).
[12] J. Williams and E. Thomas, Jr., Phys. Plasmas **14**, 063702 (2007).
[13] R. Fisher and E. Thomas, Jr., IEEE Trans. Plasma Sci. **38**, 833 (2010).
[14] R. Fisher and E. Thomas, Phys. Plasmas **18**, 113701 (2011).
[15] R. Fisher and E. Thomas, Phys. Rev. E **86**, 066403 (2012).
[16] R. A. Quinn and J. Goree, Phys. Plasmas **7**, 3904 (2000).
[17] Y. Ivanov and A. Melzer, Phys. Plasmas **12**, 072110 (2005).

[18] B. Liu, J. Goree, and Y. Feng, Phys. Rev. E **78**, 046403 (2008).
[19] R. K. Fisher, Ph.D. dissertation, Auburn University, 2012, http://hdl.handle.net/10415/3033.
[20] L. D. Landau and E. M. Lifschitz, *Statistical Physics* (Pergamon Press, New York, 1978).
[21] N. Krall and A. W. Trivelpiece, *Principles of Plasma Physics* (McGraw-Hill, New York, 1973).
[22] K. Avinash, Phys. Plasmas **17**, 123710 (2010).
[23] K. Avinash, R. Merlino, and E. Thomas, Jr., Phys. Lett. A **375**, 2854 (2011).